Journal of Photochemistry and Photobiology A: Chemistry 272 (2013) 80–89

Contents lists available at ScienceDirect

Journal of Photochemistry and Photobiology A: Chemistry

journal homepage: www.elsevier.com/locate/jphotochem

Theoretical study of cyclometalated Ru(II) dyes: Implications on the open-circuit voltage of dye-sensitized solar cells

Hitoshi Kusama*, Takashi Funaki, Kazuhiro Sayama

National Institute of Advanced Industrial Science and Technology (AIST), AIST Tsukuba Central 5, 1-1-1 Higashi, Tsukuba, Ibaraki 305-8565, Japan

ARTICLE INFO

Article history:
Received 1 July 2013
Received in revised form 26 August 2013
Accepted 4 September 2013
Available online 12 September 2013

Keywords:
Density functional theory
Dye-sensitized solar cell
Iodine
Iodide
Intermolecular interaction

ABSTRACT

A density functional theory (DFT) study was performed to elucidate why variations in the 2-phenylpyrimidinato (L) ligand of cyclometalated Ru(H_3tcterpy)L(NCS) dye affect the open-circuit photovoltage (V_{oc}) of a dye-sensitized solar cell (DSSC) using an iodine/iodide redox couple, where tcterpy represents 4,4′,4″-tricarboxy-2,2′:6′,2″-terpyridine. Neutral dye molecules interact with I_2 via the N atom of the L ligand and the S atom of the NCS ligand. Among the nine tested dyes, the intermolecular interaction strengths between the dye and I_2 correspond to the reduced V_{oc} of DSSC. Additionally, I^- interacts with oxidized dye via the L ligand and via the NCS ligand, and a second I^- bonds to the first I^-. The interaction strengths of I^- with oxidized dyes strongly correlate with the enhanced V_{oc}. The computational results suggest that the L ligand structure influences the regeneration of oxidized dye and recombination. Consequently, the L ligand structure changes V_{oc}.

1. Introduction

Since the announcement of a high solar energy conversion efficiency (η) above 7%, dye-sensitized solar cells (DSSCs) based on the concept of photosensitization of a wide band gap oxide semiconductor have attracted much attention [1]. A typical DSSC consists of three fundamental components: a sensitized photoelectrode composed of either a Ru polypyridyl complex or an organic dye-sensitized nanocrystalline n-type TiO_2 semiconductor film on transparent conductive oxide (TCO) glass, an iodine/iodide electrolyte solution, and a platinized-TCO-glass counter electrode.

Illuminating a cell with light causes the ground state of the dye to absorb a photon, and an electron is consequently transferred to a higher energy level, leading to an excited state. Then the photoexcited dye injects an electron into the TiO_2 conduction band. The injected electron percolates through the porous TiO_2 layer into the TCO glass and passes its external load to the counter electrode. Subsequently, redox mediator is reduced to I^- at the counter electrode. Finally, I^- reduces a photo-oxidized dye molecule to its original ground state (regeneration). In this way, a DSSC operates in a regenerative mode.

In addition to these desired electron transfer pathways, unwanted reactions occur simultaneously. One is recombination of injected electrons in TiO_2 with I_2 in the electrolyte [2–5]. Another is electron dye recombination in which photo-oxidized dye is regenerated by an electron from TiO_2 instead of I^- [6]. These pathways lead to a poor open-circuit photovoltage (V_{oc}) of the cell [7].

As a crucial component of a DSSC, the dye sensitizer should fulfill the following characteristics when using TiO_2 and iodine/iodide [8]. (i) It should have a high molar extinction coefficient, and the absorption spectrum should span the entire visible region and ideally the part of the near-infrared (IR) region. (ii) Anchoring groups, such as carboxyl groups, should be present to strongly bind the dye onto the TiO_2 surface for electron injection and cell stability. (iii) The excited state energy level (LUMO level) should be more positive than the conduction band edge of TiO_2, and their energy difference (ΔG_1) [9] should allow for an efficient electron transfer process between the excited dye and conduction band of the TiO_2. (iv) The oxidized state (E_{ox}, HOMO level) should be more negative than the iodine/iodide redox potential of the electrolyte, and their energy difference (ΔG_2) [9] should allow for efficient dye regeneration by I^-. (v) The structure should be optimized to avoid unfavorable dye aggregation on the TiO_2 surface. (vi) The sensitizer should be photochemically, electrochemically, and thermally stable.

Currently, **N749**, (TBA)$_3$[Ru(Htcterpy)(NCS)$_3$], where TBA represents tetra-*n*-butylammonium, is one of the most efficient and benchmark dyes to convert light into electricity with TiO_2 and iodine/iodide because the energy level of the LUMO is located appropriately above the TiO_2 conduction band [characteristic (iii)] and the absorption edge on TiO_2 is 920 nm, which is in the near-IR range [characteristic (i)] [10]. However, **N749** has an inferior incident monochromatic photon-to-electron conversion efficiency (IPCE) in the shorter wavelength region due to the absence of an effective chromophore. Additionally, the three isothiocyanato

* Corresponding author. Tel.: +81 29 861 4867.
E-mail address: h.kusama@aist.go.jp (H. Kusama).

1010-6030/$ – see front matter © 2013 Elsevier B.V. All rights reserved.
http://dx.doi.org/10.1016/j.jphotochem.2013.09.001

(NCS) ligands of **N749** negatively affect characteristic (vi) because Ru—NCS is weakly bonded. The ligands induce linkage isomers, reduce the synthetic yield, and decrease the DSSC performance because NCS is a linear ambidentate ligand [10–12].

To overcome the shortcomings of the **N749** dye and to enhance DSSC performance, we have examined terpyridyl Ru(II) complexes Ru(H_3tcterpy)L(NCS), where L is a bidentate ligand instead of two NCS ligands [13–15]. We have synthesized a new cyclometalated Ru(II) complex, **FT89**, where L is 2-(2,4-bistrifluoromethylphenyl)pyrimidinato ligand (Chart 1) [9]. **FT89** exhibits an efficient panchromatic sensitization over the entire visible wavelength range, which extends into the near-IR region. Compared to **N749**, **FT89** improves the short-circuit photocurrent density (J_{sc}) due to the higher molecular excitation coefficient [characteristic (i)] and IPCE values by tuning of the HOMO energy level and ΔG_2 with a strongly electron-withdrawing trifluoromethyl (CF_3) group on the strong σ-donating cyclometalating 2-phenylpyrimidinato ligand. Consequently, a DSSC sensitized with **FT89** shows a higher η value than that of the **N749** benchmark under same cell fabrication conditions.

The η (as a percentage) for a solar cell under 100 mW cm^{-2} (AM 1.5) irradiation is given by J_{sc}, V_{oc}, and fill factor of the cell (ff) as [7]

$$\eta = J_{sc} V_{oc} ff (\%) \quad (1)$$

Thus, both J_{sc} and V_{oc} must be increased to enhance η. Although the mechanism of J_{sc} to alter has been fully elucidated, the origin of effect on V_{oc} induced by 2-phenylpyrimidine derivatives as a bidentate L ligand for [Ru(H_3tcterpy)L(NCS)] dye remains unknown.

Modern quantum chemical calculations, such as DFT and its time dependent extension (TD-DFT), provide the theoretical/computational framework to understand and predict the desired properties of individual dyes, such as HOMO, LUMO, HOMO–LUMO gap, and adsorption spectrum [16–18], and may save substantial experimental time and resources. Recently, we studied the effect of side groups in a Ru(H_2dcbpy)$_2$(NCS)$_2$ sensitizer (**N3**, dcbpy = 4,4′-dicarboxy-2,2′-bipyridine), which is the other benchmark dye in DSSCs, on the interactions with iodine species using DFT. Our results suggest that the stronger the interaction between a neutral dye molecule and an I_2 molecule, the more readily the unfavorable recombination reaction of electrons with an acceptor in the electrolyte is catalyzed, reducing the V_{oc} value of DSSC [19]. Although many theoretical reports have examined bipyridyl isothiocyanato Ru dyes [19–23] and organic dyes [24–28], to the best of our knowledge, the intermolecular interactions between iodine species and terpyridyl isothiocyanato Ru dyes in relation to recombination have yet to be studied theoretically.

Herein, nine isolated Ru(H_3tcterpy)L(NCS) complexes (L = 2-phenylpyrimidinato ligands, Chart 1), including **FT89**, and their intermolecular interactions with iodine species in the redox couple are investigated via quantum chemical calculations at the DFT level. On the basis of the DFT results (i.e., geometrical features, charge distributions, and interaction energies), we discuss how variations in the 2-phenylpyrimidinato bidentate ligand with F and CF_3 substituents in cyclometalated Ru(II) terpyridyl complex influence the V_{oc} values of actual DSSCs. Our findings have implications on the design of dye and dye/electrolyte structures, and should improve DSSC performance.

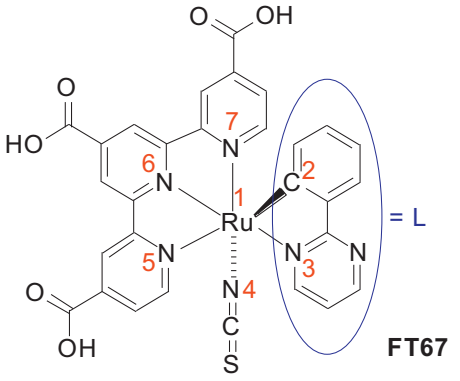

dye	L ligand
FT10	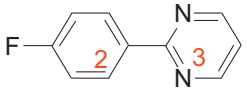
FT57	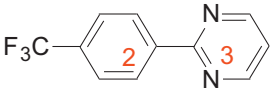
FT99	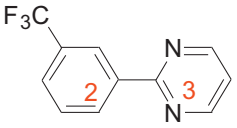
FT111	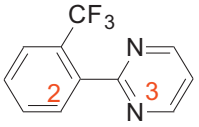
FT89	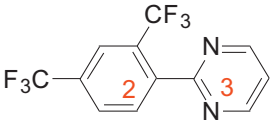
FT100	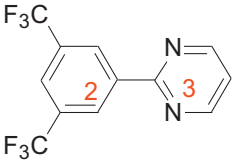
FT104	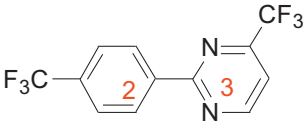
FT124	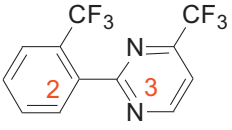

Chart 1. Constitutional formulas of the **FT** complexes.

2. Experimental

DSSC preparation and photovoltaic characterization were conducted as previously described [9]. TiO_2 pastes were obtained from Sumitomo Osaka Cement Co., Ltd. TiO_2 films were fabricated on TCO glass (Nippon Sheet Glass Co., Japan, F-doped SnO_2 layer) using a screen printing method. The resulting films were composed of a 2.5×10^{-5}-m thick transparent layer and a 0.6×10^{-5}-m thick scattering layer. The TiO_2 films were heated 798 K for 2 h in air, and allowed to cool to 393 K before dipping in 0.1 mol dm^{-3} HCl at 353 K for 2 h. After rinsing with water and ethanol, the TiO_2 photoelectrodes were immersed into an ethanol solution of dye for 22 h at 298 K. The concentration of Ru(II) complexes was 2×10^{-4} mol dm^{-3} and the solution contained 4×10^{-4} mol dm^{-3}

tetra-*n*-butylammonium hydroxide. To suppress dye aggregation on the TiO_2 surface [29], deoxycholic acid was used as a co-adsorbate at a concentration of 4×10^{-2} mol dm^{-3}.

Photoelectrochemical measurements were performed using a sandwich-type two-electrode solar cell, which consisted of a dye-coated TiO_2 electrode, a platinum film counter electrode, a 6×10^{-5}-m thick polypropylene spacer film, and an electrolyte solution. The electrolyte solution was composed of 0.6 mol dm^{-3} of 1,2-dimethyl-3-propylimidazolium iodide, 0.1 mol dm^{-3} of LiI, 0.05 mol dm^{-3} of I_2, and 0.5 mol dm^{-3} of 4-*tert*-butylpyridine in acetonitrile. The solar cell performance was then measured under simulated solar light (AM 1.5, 100 mW cm^{-2}). The current density–voltage curve was measured using a digital source meter and a data acquisition system. The apparent cell area of the TiO_2 photoelectrode was 0.25 cm^2 (0.5 cm × 0.5 cm).

3. Theoretical calculations

DFT calculations were performed using the Gaussian 09 program at the Research Center for Computational Science, Okazaki, Japan and the Gaussian 09W program on personal computers [30]. Geometry optimizations were carried out at the pure generalized gradient approximation (GGA) DFT level using the PBEPBE functional [31], which has been used to study weak-interacting systems [32]. The geometries were also fully optimized at the hybrid DFT level by the mPW1PW91 functional, which combined the Perdew–Wang 1991 exchange functional as modified by Adamo and Barone (mPW1) with the Perdew and Wang's 1991 gradient-corrected correlation functional (PW91) [33]. This combination improves the well-known deficiency in the long-range behavior of the DFT functional, which is especially important when studying noncovalent intermolecular interactions [29,33–35]. It has been reported that the mPW1PW91 functional provides appropriate results for **N749** structures [16]. For H, C, N, O, F, and S atoms, a mixed basis set where 6-31G(d,p) basis functions [36] was employed, while the Los Alamos effective core potential (ECP) plus Hay–Wadt double-zeta basis set (LanL2DZ ECP) [37–40] was used for Ru and I. This mixed basis set has accurately described the geometrical parameters in **N749** dye [16–18,29].

The solvent effects of acetonitrile were modeled using a conductor-like polarizable continuum model (C-PCM) [41] within the self-consistent reaction field (SCRF) theory. In the SCRF calculations, the dielectric constant of acetonitrile was 35.688. All of the species in acetonitrile had non-imaginary frequency geometries, confirming that the optimized structures corresponded to real minima on the whole potential energy surface. The intermolecular interaction energies were determined as energy differences between the sum of the isolated monomers and the complex.

Hirshfeld [42–44] and Natural population analysis (NPA) [45,46] with the CPCM SCRF model was conducted on the optimized geometries.

4. Results

4.1. DSSC performance

Table 1 lists the results of the DSSC performance when illuminating with 100 mW cm^{-2}. Among the nine tested **FT** dyes, **FT67** displayed the lowest V_{oc} value (0.55 V). The F substituent at position 4 in the phenyl group of L ligand increased V_{oc} (**FT10**, 0.61 V). Replacing the F group by CF_3, enhanced V_{oc} at **FT57** (0.62 V). An additional CF_3 substituent (**FT89** and **FT104**) further improved V_{oc} (0.69 V and 0.67 V, respectively).

For the three isomers possessing one CF_3 substituent on L ligand, **FT99** showed the highest V_{oc} (0.64 V). For the isomers with two CF_3 groups, the value of V_{oc} increased in the following order: **FT104** = **FT124** < **FT89** < **FT100**.

Table 1
DSSC performances and E_{ox} potentials.

Dye	V_{oc} (V)	J_{sc} (mA cm^{-2})	*ff*	η (%)	E_{ox} (V vs. SCE)
FT67	0.55	7.9	0.72	3.1	0.42
FT10	0.61	15.6	0.69	6.5	0.48
FT57	0.62	20.1	0.66	8.2	0.49
FT99	0.64	21.9	0.63	8.9	0.51
FT111	0.62	20.9	0.65	8.4	0.49
FT89	0.69	22.0	0.68	10.2	0.52
FT100	0.70	19.6	0.66	9.1	0.56
FT104	0.67	21.6	0.67	9.6	0.55
FT124	0.67	21.7	0.65	9.4	0.53

4.2. Structures of neutral dyes

Our theoretical study began with the neutral species in a singlet electronic state and a total charge of 0. Table 2 lists the main bond distances and angles of the optimized Ru(H_3tcterpy)L(NCS) structures. The central Ru and six atoms bonded to the Ru were labeled with red-numbers, as illustrated in **FT67** of Chart 1. The structure of the L ligand significantly influenced the distances of the Ru—C2, Ru—N3, and Ru—N4 bonds. For **FT100**, substitution of CF_3 at position 3 in the phenyl group elongated the Ru—C2 bond distance over 0.04 Å, but shortened the Ru—N3 and Ru—N4 ones compared to **FT99**. Similarly, the CF_3 substituent reduced the Ru—N3 distances by 0.02 Å for **FT111** and **FT89** compared to **FT67** and **FT57**, respectively. Changing the L ligand had a negligible effect on the geometrical parameters of the H_3tcterpy ligand. Regardless of the DFT functional, the bond distances of Ru—N5, Ru—N6, and Ru—N7, and the bond angle of N5—Ru—N7 were nearly the same among the nine complexes.

Table 2 lists the energy of the HOMO level. The relative order among the nine complexes at the PBEPBE level mostly agreed with that at the mPW1PW91 level. They are also in line with the relative order of measured E_{ox} in Table 1, indicating the accuracy of the calculations (Fig. S1). **FT67** and **FT100** had the highest and the lowest energies of the HOMO level, respectively.

Table 3 lists the charge distributions of the neutral dyes determined by Hirshfeld and NPA. The distributed atomic charge using Hirshfeld and NPA became negative in the order of H_3tcterpy < Ru < L < NCS. Although the values differed according to the analysis method and DFT functional, the relative orders of the atomic charges on the L, NCS, and H_3tcterpy ligands among the nine dyes were analogous. When the H atom at position 4 for the phenyl group of L ligand (**FT67**) was substituted by a F atom (**FT10**), the atomic charge on the L ligand became more negative due to the electron-withdrawing effect. Likewise, dyes with two CF_3 groups, such as **FT89**, **FT100**, **FT104**, and **FT124**, were more negatively charged on the L ligand, but more positively charged on the NCS and H_3tcterpy ones than monosubstituted analogs, such as **FT57**, **FT99**, and **FT111**.

4.3. Structures of neutral dye interactions with I_2

Next, we geometrically optimized the dye-I_2 species with a total charge of 0 and multiplicity of 1. I_2 interacted via the N atom of the L ligand and the S atom of the NCS ligand (Fig. S2). Table 4 lists the corresponding intermolecular interaction energies (E), atomic charges on the I_2 molecule, and the selected bond distances. Regardless of the dye and DFT functional, the E values for the intermolecular interaction via the S atom of the NCS ligand were larger than those via the N atom of the L. The stronger the dye interacted with an I_2 molecule, the more charge transfer occurred from the donor (dye)

Table 2
Selected bond distances (Å), bond angles (deg), and energies of the HOMO level (eV) for neutral dyes.

Functional	Parameter	FT67	FT10	FT57	FT99	FT111	FT89	FT100	FT104	FT124
PBEPBE	Ru–C2	2.042	2.040	2.039	2.036	2.037	2.034	2.077	2.038	2.035
	Ru–N3	2.129	2.129	2.128	2.128	2.101	2.099	2.108	2.117	2.091
	Ru–N4	2.172	2.167	2.166	2.167	2.171	2.166	2.151	2.166	2.172
	Ru–N5	2.071	2.072	2.073	2.074	2.073	2.075	2.073	2.075	2.075
	Ru–N6	1.952	1.953	1.954	1.954	1.959	1.960	1.963	1.957	1.962
	Ru–N7	2.072	2.073	2.074	2.074	2.074	2.076	2.073	2.075	2.076
	C2–Ru–N4	169.4	169.5	169.5	169.6	170.0	170.1	168.4	169.8	170.3
	N3–Ru–N6	175.5	175.5	175.5	175.7	176.1	176.0	173.5	175.5	176.2
	N5–Ru–N7	159.5	159.5	159.4	159.4	159.2	159.2	159.3	159.3	159.1
	HOMO	−4.625	−4.655	−4.685	−4.699	−4.680	−4.734	−4.775	−4.736	−4.732
mPW1PW91	Ru–C2	2.033	2.031	2.032	2.028	2.029	2.026	2.077	2.031	2.028
	Ru–N3	2.127	2.127	2.127	2.127	2.101	2.100	2.109	2.119	2.094
	Ru–N4	2.177	2.172	2.171	2.172	2.176	2.170	2.148	2.170	2.175
	Ru–N5	2.077	2.079	2.079	2.080	2.080	2.081	2.080	2.081	2.081
	Ru–N6	1.952	1.953	1.954	1.954	1.958	1.960	1.965	1.956	1.961
	Ru-N7	2.078	2.079	2.080	2.080	2.080	2.082	2.080	2.081	2.082
	C2–Ru–N4	170.8	170.9	170.9	171.0	171.3	171.4	169.6	171.0	171.5
	N3–Ru–N6	175.2	175.2	175.2	175.5	175.6	175.6	174.4	175.3	175.7
	N5–Ru–N7	159.2	159.1	159.1	159.1	158.9	158.9	159.0	159.0	158.8
	HOMO	−5.529	−5.586	−5.618	−5.639	−5.609	−5.688	−5.739	−5.673	−5.667

Table 3
Charge distributions of the neutral Ru(H_3tcterpy)L(NCS) species.

Functional	Method		FT67	FT10	FT57	FT99	FT111	FT89	FT100	FT104	FT124
PBEPBE	Hirshfeld	Ru	0.0374	0.0367	0.0368	0.0372	0.0360	0.0354	0.0330	0.0386	0.0380
		L	0.0057	−0.0133	−0.0294	−0.0337	−0.0230	−0.0573	−0.0534	−0.0670	−0.0621
		NCS	−0.6235	−0.6206	−0.6189	−0.6190	−0.6198	−0.6155	−0.5962	−0.6166	−0.6175
		H_3tcterpy	0.5792	0.5961	0.6099	0.6140	0.6053	0.6354	0.6142	0.6437	0.6401
	NPA	Ru	0.0489	0.0465	0.0455	0.0446	0.0459	0.0426	0.0177	0.0459	0.0468
		L	0.0347	0.0172	0.0041	0.0010	0.0132	−0.0168	−0.0280	−0.0292	−0.0217
		NCS	−0.6552	−0.6522	−0.6508	−0.6513	−0.6535	−0.6492	−0.6359	−0.6496	−0.6522
		H_3tcterpy	0.5716	0.5886	0.6011	0.6057	0.5944	0.6234	0.6462	0.6329	0.6272
mPW1PW91	Hirshfeld	Ru	−0.0018	−0.0019	−0.0022	−0.0016	−0.0039	−0.0041	−0.0048	−0.0016	−0.0032
		L	−0.0202	−0.0404	−0.0511	−0.0555	−0.0451	−0.0757	−0.0794	−0.0804	−0.0756
		NCS	−0.6640	−0.6611	−0.6597	−0.6597	−0.6597	−0.6554	−0.6309	−0.6570	−0.6569
		H_3tcterpy	0.6849	0.7023	0.7117	0.7153	0.7071	0.7333	0.7129	0.7376	0.7341
	NPA	Ru	0.0423	0.0409	0.0398	0.0390	0.0382	0.0358	0.0144	0.0379	0.0367
		L	−0.0074	−0.0255	−0.0337	−0.0365	−0.0244	−0.0502	−0.0695	−0.0575	−0.0495
		NCS	−0.6960	−0.6933	−0.6921	−0.6925	−0.6936	−0.6897	−0.6718	−0.6906	−0.6920
		H_3tcterpy	0.6611	0.6779	0.6861	0.6900	0.6798	0.7041	0.7269	0.7102	0.7048

Table 4
Intermolecular interaction energies (E of I_2, kcal mol^{-1}), atomic charges on the I_2 (e), and selected bond distances (Å) for the neutral dye–I_2 species.

Functional	Site		FT67	FT10	FT57	FT99	FT111	FT89	FT100	FT104	FT124
PBEPBE	L	E	−12.93	−12.96	−12.19	−12.17	−7.32	−6.61	−11.09	−6.04	−5.65
		Hirshfeld[a]	−0.3508	−0.3521	−0.3366	−0.3333	−0.3193	−0.3018	−0.3220	−0.2876	−0.3942
		NPA[b]	−0.2883	−0.2884	−0.2765	−0.2750	−0.2639	−0.2486	−0.2691	−0.2528	−0.4497
		N···I distance	2.543	2.536	2.552	2.555	2.625	2.641	2.580	2.768	3.943
		I—I distance	3.013	3.014	3.006	3.005	2.993	2.984	2.999	2.977	3.072
	NCS	E	−21.87	−21.79	−21.70	−21.67	−21.65	−21.51	−21.00	−21.50	−21.43
		Hirshfeld[a]	−0.5560	−0.5532	−0.5517	−0.5498	−0.5547	−0.5553	−0.5407	−0.5382	−0.5355
		NPA[b]	−0.5280	−0.5256	−0.5233	−0.5222	−0.5229	−0.5185	−0.5047	−0.5154	−0.5141
		S···I distance	2.843	2.843	2.841	2.843	2.839	2.838	2.845	2.846	2.846
		I—I distance	3.115	3.113	3.112	3.111	3.112	3.109	3.100	3.107	3.106
mPW1PW91	L	E	−8.17	−7.69	−7.38	−7.08	−2.72	−2.07	−6.51	−0.85	−1.12
		Hirshfeld[a]	−0.3064	−0.2783	−0.2847	−0.2649	−0.2313	−0.2001	−0.2671	−0.0239	−0.0016
		NPA[b]	−0.2281	−0.2093	−0.2120	−0.1993	−0.1690	−0.1463	−0.2001	−0.0250	−0.0084
		N···I distance	2.525	2.567	2.552	2.580	2.657	2.715	2.574	3.467	4.627
		I—I distance	2.960	2.947	2.949	2.941	2.919	2.905	2.940	2.840	2.832
	NCS	E	−17.76	−17.73	−17.57	−17.68	−17.48	−17.51	−16.70	−17.50	−17.39
		Hirshfeld[a]	−0.5320	−0.5319	−0.5380	−0.5452	−0.5338	−0.5398	−0.5116	−0.5438	−0.5281
		NPA[b]	−0.4803	−0.4786	−0.4788	−0.4809	−0.4773	−0.4775	−0.4588	−0.4785	−0.4733
		S···I distance	2.786	2.786	2.786	2.784	2.786	2.787	2.793	2.784	2.785
		I—I distance	3.067	3.066	3.066	3.067	3.065	3.065	3.054	3.066	3.063

[a] Atomic charge by Hirshfeld method.
[b] Atomic charge by NPA.

to the acceptor (I_2), and the more negatively the atomic charge on the I_2 varied from 0. The larger the *E* values of I_2, the more negative the atomic charge in Table 4.

Compared to isolated I_2 bonds (2.862 Å at the PBEPBE level and 2.833 Å at the mPW1PW91 level), the elongated intramolecular I—I bonds implied that the I_2 monomer bonds were weakened in the dye-I_2 species. For interactions via the N atom of L ligand, the results at both the PBEPBE and mPW1PW91 levels indicated nearly identical relative orders of the *E* values for nine complexes, and were consistent with shorter intermolecular N···I distances, elongated intramolecular I—I distances, and increased negative charges on the I_2. A similar relationship between the *E* values and I—I bond distances occurred for the interactions via the S atom of the NCS ligand.

4.4. Structures of oxidized dyes

After an electron was injected the TiO_2 conduction band, the dye became cationic with a monopositive charge (+1) in the doublet electronic spin state. Table S1 lists the main bond distances and angles of the optimized dye^+ species. The substituent effects of the L ligand on the main bond distances and angles resembled those for the neutral dyes (Table 2). Table 5 lists the charge distribution of the oxidized dye determined by Hirshfeld and NPA. The effects of the substituents on the charge distributions of the oxidized dyes were analogous to those for the neutral dyes (Table 3). The atomic charges on the L ligand for oxidized **FT10** were less positive than those for **FT67** due to the F atom at the phenyl group, while those on the NCS one were less negative. Compared to oxidized **FT67**, a CF_3 substituent for oxidized **FT57**, **FT99**, and **FT111** caused the atomic charge on the L ligand to be less positive, while that on the NCS was more positive. The atomic charges on L and NCS for oxidized **FT89**, **FT100**, **FT104**, and **FT124** became less positive and less negative than oxidized **FT57**, **FT99**, and **FT111** due to two CF_3 substituents.

4.5. Structures of oxidized dye interactions with iodides

The interaction of a dye cation with the redox mediator (I^-) controlled the regeneration of the oxidized dye. Although several models have been proposed for the regeneration process based on experimental kinetics measurements, the two mechanisms below were assumed. The first one is a two-step mechanism proposed by Clifford and co-workers [6,47]:

$$Dye^+ + I^- \rightarrow [Dye^+ \cdot I^-] \quad (2)$$

$$[Dye^+ \cdot I^-] + I^- \rightarrow [Dye \cdot I_2^-] \rightarrow Dye^0 + I_2^{\bullet -} \quad (3)$$

$$2I_2^{\bullet -} \rightarrow I^- + I_3^- \quad (4)$$

The formation of the first intermediate (Eq. (2)) is kinetically fast. The subsequent reaction of the intermediate with a second iodide ion (Eq. (3)) is much slower, and the rate-determining step of the overall regeneration reaction.

The second mechanism proposed by Gardner and co-workers does not require a reaction between a second iodide species and the first intermediate [6,48]:

$$Dye^+ + I^- \rightarrow [Dye^+ \cdot I^-] \rightarrow Dye^0 + I^{\bullet} \quad (5)$$

$$I^{\bullet} + I^- \rightarrow I_2^{\bullet -} \quad (6)$$

In this one-step mechanism, the $[Dye^+ \cdot I^-]$ intermediate dissociates into a reduced dye and a free iodine radical (Eq. (5)).

Consequently, the interaction of oxidized dye with an I^- (Eqs. (2) and (5)) and the subsequent interaction with a second I^- (Eq. (3)) were investigated theoretically. The structures of the dye interacting with I^- via the N atom of the L ligand and via the S atom of the NCS ligand were optimized with a total charge of 0 and a multiplicity of 2 (Fig. S3). Table 6 lists the *E* values of I^- with the oxidized dye species and the atomic charges on the I atom determined by Hirshfeld, and NPA. Regardless of the interaction site and DFT functional, the relative orders of *E* for the nine dyes were similar. **FT100** (**FT67**) had the strongest (weakest) intermolecular interaction with I^-. The atomic charge on the I atom became less negative and approached 0 as the *E* value increased, indicating more charge transfer from I^- to oxidized dye as the I atomic charge approached 0. The N···I distances for dye^+–I^- species were around 5 Å, which were much longer than those for the neutral dye–I_2 species in Table 4. Instead, I^- seemed to coordinate with the π system of the L ligand. The higher the *E* values, the shorter the intermolecular S···I bond distances (Table 6).

Next the dye^+–I^- species interacting with a second I^- was optimized in the doublet electronic spin state with a total charge of −1 (Fig. S4). All of the dyes were successfully optimized as a dye^+–I^-–I^- species, demonstrating that the two-step regeneration model (Eq. (3)) is applicable for the Ru(H_3tcterpy)L(NCS) sensitizers in this study. Regardless of the DFT functional and interaction site, the *E* values for a second I^- with dye^+–I^- and for I_2^- with dye were directly proportional (Table 7). Similar to the findings of dye^+–I^- species in Table 6, the atomic charge on I_2^- became less negative as the *E* values increased. The interactions with the second I^- generally elongated the intermolecular S···I bonds of dye^+–I^- species (Table 6). The formed I—I bond distances were very close to the optimized bond distance in an isolated I_2^- molecule (3.410 Å at the PBEPBE and 3.364 Å at the mPW1PW91 level). According to the reports of Privalov and co-workers [20,24], these observations suggest that the role of the second I^- in the two-step regeneration mechanism is to generate the $I_2^{\bullet -}$ species at the final step from $[Dye \cdot I_2^-]$ species (Eq. (3)). The relative orders of the *E* values among the nine dyes in Table 7 were approximately same regardless of DFT functional, interacting site, and the number of I^-. **FT100** (**FT67**) exhibited the strongest (weakest) intermolecular interaction with iodides, corresponding with the results of dye^+–I^- species.

5. Discussion

Substitutions of one or two H atoms in the 2-pheylpridiminato (L, Chart 1) ligand of **FT** dye with F or CF_3 groups enhances V_{oc} of DSSC using I^-/I_3^- redox couple from 0.55 V (**FT67**) up to 0.70 V (**FT100**, Table 1). The DFT study indicates that the derivatives drastically change both their structure and interaction strengths with iodine species such as I_2 and I^-.

O'Regan and co-worker have noted that the mechanism to accelerate recombination in DSSCs must involve a combination of the strength of the I_2 binding site and the proximity to the TiO_2 surface, and may involve catalysis of the reduction by stabilization of an intermediate [49,50]. They have also noted that dye–I_2 binding increases the amount of "free" I_2 in the TiO_2 pore structure even in standard electrolytes and may influence recombination [5]. Although the mechanistic details remain unknown and further research is needed, they have presented compelling evidence that certain dye molecules catalyze electron recombination with the electrolyte in DSSC due to their binding ability with the I_2 molecule. Acceleration of recombination, in which electrons in TiO_2 are transferred back to the I_2 in the electrolyte [2–4,26], lowers V_{oc}.

Actually, we found a good correlation between V_{oc} in Table 1 and *E* of I_2 in Table 4 (Fig. 1). V_{oc} increases as *E* of I_2 for the neutral dye–I_2 species decreases. The correlation coefficients are −0.58 for the L at the PBEPBE, −0.85 for the NCS at the PBEPBE, −0.57 for the L at the mPW1PW91, and −0.69 for the NCS site at the mPW1PW91 levels. Thus variation of the 2-phenylpyrimidinato bidentate ligand in an **FT** dye affects V_{oc} of DSSC because the ligand changes the

Table 5
Charge distributions of the oxidized Ru(H_3tcterpy)L(NCS) species.

Functional	Method		FT67	FT10	FT57	FT99	FT111	FT89	FT100	FT104	FT124
PBEPBE	Hirshfeld	Ru	0.1044	0.1052	0.1066	0.1075	0.1064	0.1077	0.1064	0.1069	0.1068
		L	0.2520	0.2256	0.1973	0.1924	0.2068	0.1599	0.1563	0.1655	0.1725
		NCS	−0.3581	−0.3464	−0.3324	−0.3306	−0.3400	−0.3183	−0.2948	−0.3195	−0.3253
		H_3tcterpy	1.0008	1.0148	1.0274	1.0296	1.0254	1.0491	1.0299	1.0460	1.0448
	NPA	Ru	0.1561	0.1580	0.1592	0.1608	0.1604	0.1622	0.1448	0.1565	0.1589
		L	0.2703	0.2431	0.2156	0.2106	0.2289	0.1827	0.1558	0.1874	0.1976
		NCS	−0.3891	−0.3771	−0.3623	−0.3610	−0.3724	−0.3498	−0.3318	−0.3491	−0.3575
		H_3tcterpy	0.9628	0.9760	0.9875	0.9896	0.9831	1.0049	1.0312	1.0051	1.0011
mPW1PW91	Hirshfeld	Ru	0.1324	0.1355	0.1355	0.1376	0.1358	0.1377	0.1412	0.1349	0.1358
		L	0.2420	0.2111	0.1967	0.1919	0.2070	0.1692	0.1583	0.1720	0.1817
		NCS	−0.5041	−0.4916	−0.4838	−0.4844	−0.4925	−0.4751	−0.4457	−0.4702	−0.4799
		H_3tcterpy	1.1285	1.1438	1.1501	1.1536	1.1484	1.1665	1.1449	1.1622	1.1612
	NPA	Ru	0.2862	0.2916	0.2907	0.2941	0.2940	0.2956	0.2845	0.2860	0.2901
		L	0.2262	0.1947	0.1821	0.1776	0.1957	0.1598	0.1251	0.1617	0.1743
		NCS	−0.5585	−0.5464	−0.5384	−0.5396	−0.5499	−0.5329	−0.5101	−0.5247	−0.5371
		H_3tcterpy	1.0461	1.0601	1.0656	1.0679	1.0602	1.0775	1.1006	1.0769	1.0727

Table 6
Intermolecular interaction energies (E of I^-, kcal mol^{-1}), atomic charges on the I atom (e), and bond distances (Å) for the dye$^+$–I^- species.

Functional	Site		FT67	FT10	FT57	FT99	FT111	FT89	FT100	FT104	FT124
PBEPBE	L	E	−4.24	−4.45	−4.56	−4.55	−4.47	−4.80	−5.03	−4.67	−4.91
		Hirshfeld[a]	−0.7873	−0.7753	−0.7616	−0.7577	−0.7606	−0.7382	−0.7197	−0.7353	−0.7366
		NPA[b]	−0.8691	−0.8559	−0.8426	−0.8367	−0.8401	−0.8171	−0.7954	−0.8151	−0.8198
		N···I distance	4.940	4.887	4.920	4.922	5.084	5.080	4.859	5.028	4.785
	NCS	E	−5.05	−5.12	−5.78	−5.94	−5.42	−7.03	−7.01	−6.62	−6.44
		Hirshfeld[a]	−0.6083	−0.5412	−0.5238	−0.4999	−0.5040	−0.5563	−0.4774	−0.4889	−0.4893
		NPA[b]	−0.6053	−0.5584	−0.5422	−0.5225	−0.5280	−0.5563	−0.4991	−0.5123	−0.5133
		S···I distance	3.373	3.310	3.285	3.255	3.267	3.294	3.236	3.242	3.246
mPW1PW91	L	E	−2.84	−2.89	−2.93	−2.98	−3.00	−3.05	−3.22	−3.10	−3.06
		Hirshfeld[a]	−0.8915	−0.8903	−0.8901	−0.8975	−0.8940	−0.8918	−0.8900	−0.8856	−0.8845
		NPA[b]	−0.9785	−0.9782	−0.9779	−0.9792	−0.9787	−0.9781	−0.9772	−0.9772	−0.9765
		N···I distance	4.844	4.670	4.586	5.137	4.855	4.801	4.606	4.626	4.649
	NCS	E	1.75	0.44	−0.05	−0.50	0.62	−1.37	−2.22	−1.37	−0.99
		Hirshfeld[a]	−0.4515	−0.4763	−0.4475	−0.4721	−0.4659	−0.4679	−0.4426	−0.4476	−0.4391
		NPA[b]	−0.4533	−0.4603	−0.4501	−0.4568	−0.4444	−0.4511	−0.4342	−0.4452	−0.4438
		S···I distance	3.111	3.122	3.114	3.118	3.107	3.117	3.104	3.110	3.113

[a] Atomic charge by Hirshfeld method.
[b] Atomic charge by NPA.

Table 7
Intermolecular interaction energies (E, kcal mol^{-1}), atomic charges on the I_2^- (e), and selected bond distances (Å) for the dye$^+$–I^-–I^- species.

Functional	Site		FT67	FT10	FT57	FT99	FT111	FT89	FT100	FT104	FT124
PBEPBE	L	E(second I^-)	−4.67	−5.32	−6.06	−6.36	−5.95	−7.11	−7.89	−7.36	−6.99
		E(I_2^-)	−8.91	−9.76	−10.62	−10.90	−10.42	−11.92	−12.93	−12.03	−11.90
		Hirshfeld[a]	−0.9140	−0.9139	−0.9107	−0.9099	−0.9109	−0.9101	−0.9070	−0.9070	−0.9084
		NPA[b]	−0.9878	−0.9876	−0.9866	−0.9864	−0.9865	−0.9860	−0.9844	−0.9854	−0.9861
		N···I distance	4.421	4.399	4.522	4.582	4.280	4.346	4.285	4.464	4.287
		I—I distance	3.407	3.407	3.406	3.407	3.408	3.406	3.405	3.406	3.403
	NCS	E(second I^-)	−3.67	−4.42	−4.73	−4.88	−4.82	−4.73	−5.57	−5.11	−5.08
		E(I_2^-)	−8.72	−9.54	−10.51	−10.82	−10.24	−11.76	−12.57	−11.73	−11.52
		Hirshfeld[a]	−1.0667	−1.0639	−0.9818	−0.9813	−0.9814	−0.9591	−1.0275	−1.0265	−1.0374
		NPA[b]	−1.1070	−1.1035	−1.0425	−1.0420	−1.0412	−1.0219	−1.0827	−1.0780	−1.0875
		S···I distance	3.790	3.803	4.216	4.218	4.222	4.414	3.798	3.925	3.850
		I—I distance	3.510	3.507	3.454	3.453	3.452	3.435	3.492	3.484	3.492
mPW1PW91	L	E(second I^-)	−0.08	−1.36	−2.02	−2.38	−1.57	−3.41	−4.64	−3.39	−3.06
		E(I_2^-)	−2.92	−4.26	−4.95	−5.37	−4.57	−6.46	−7.87	−6.49	−6.12
		Hirshfeld[a]	−0.9309	−0.9301	−0.9308	−0.9316	−0.9295	−0.9268	−0.9255	−0.9408	−0.9303
		NPA[b]	−0.9931	−0.9929	−0.9931	−0.9929	−0.9926	−0.9920	−0.9915	−0.9946	−0.9933
		N···I distance	5.051	5.067	4.996	4.900	4.852	4.892	4.522	5.137	4.693
		I—I distance	3.361	3.361	3.360	3.361	3.362	3.360	3.361	3.364	3.362
	NCS	E(second I^-)	−4.42	−4.44	−4.73	−4.70	−4.96	−4.70	−5.41	−4.75	−4.87
		E(I_2^-)	−2.67	−4.00	−4.79	−5.20	−4.33	−6.06	−7.63	−6.12	−5.86
		Hirshfeld[a]	−0.9395	−0.9391	−0.9426	−0.9423	−0.9388	−0.9394	−0.9388	−0.9457	−0.9534
		NPA[b]	−0.9934	−0.9936	−0.9921	−0.9930	−0.9930	−0.9951	−0.9913	−0.9972	−0.9928
		S···I distance	5.027	4.901	6.227	5.499	5.041	4.728	6.574	4.725	5.961
		I—I distance	3.363	3.363	3.362	3.361	3.362	3.361	3.364	3.364	3.363

[a] Atomic charge by Hirshfeld method.
[b] Atomic charge by NPA.

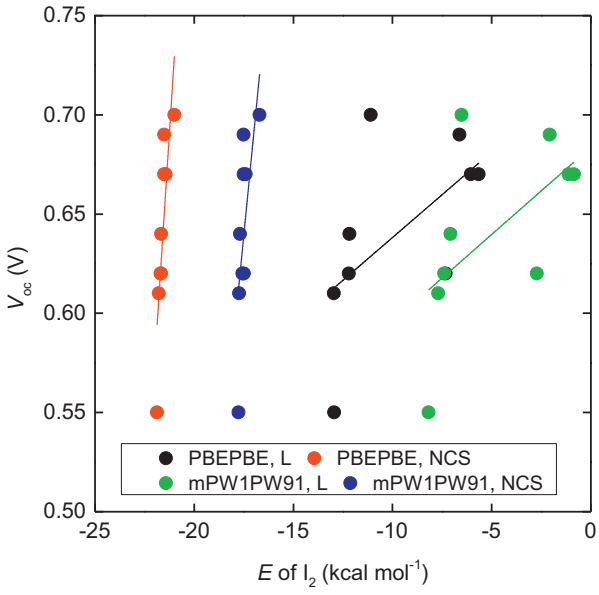

Fig. 1. Correlation between V_{oc} of the DSSC and E of I_2 for the neutral dye–I_2 species.

ability of the neutral dye to bind an I_2 molecule and the extent of catalysis for the recombination reaction of electrons with the I_2 in the electrolyte.

Jennings and co-workers have reported that a cell with Ru(H_2dcbpy)(4,4′-diamino-2,2′-bipyridine)(NCS)$_2$ (**Z960**) sensitizer decreases V_{oc} by 17% compared to a cell employing Ru(H_2dcbpy)(4,4′-dinonyl-2,2′-bipyridine)(NCS)$_2$ (**Z907**) [51]. Characterization results suggest that this decrease is due to a faster charge recombination with the electrolytes and is not related to a lower sensitizer regeneration yield for the cell using **Z960**. However, they noted that some contribution to the overall recombination flux under illumination from the electron transfer to the oxidized sensitizer molecules cannot be ruled out entirely. Li and co-worker have also reported that V_{oc} of the cell using Ru(dcbpy)(4,4′-dimethyl-2,2′-bipyridine)$_2$ (**Z995**) dye is lower than that using TBA_2[Ru(Hdcbpy)$_2$(NCS)$_2$] (**N719**) dye [5];

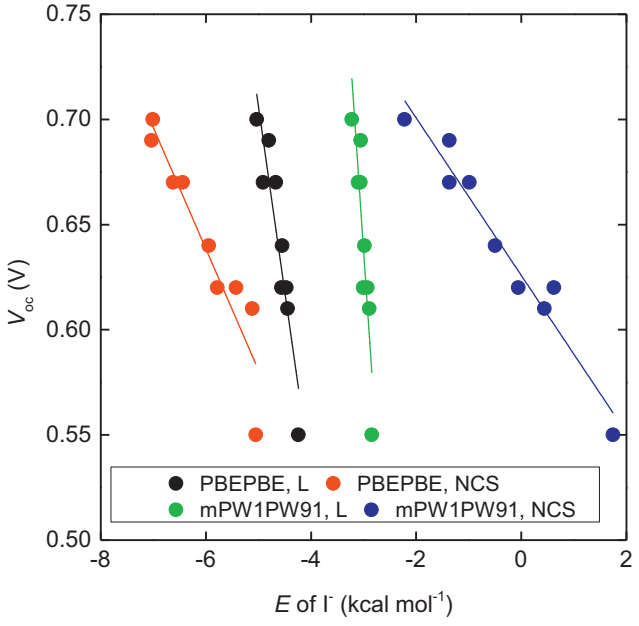

Fig. 2. Correlation between V_{oc} of the DSSC and E of I^- for the dye$^+$–I^- species.

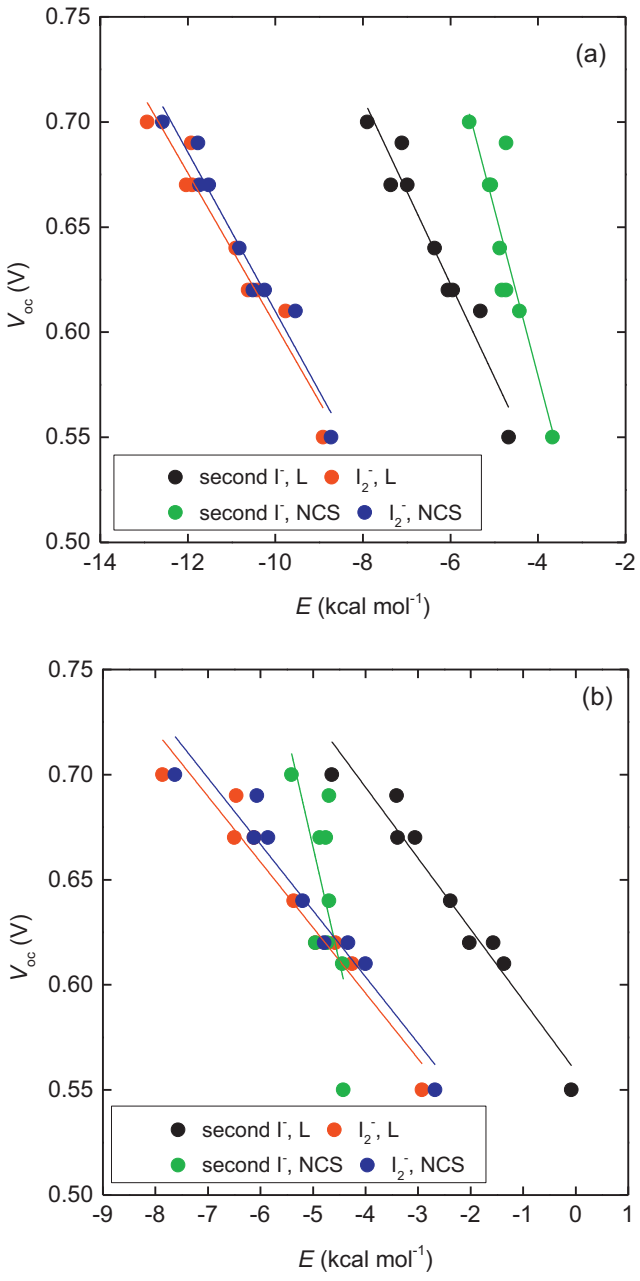

Fig. 3. Correlation between V_{oc} of the DSSC and E of iodide for the dye$^+$–I^-–I^- species at the (a) PBEPBE and (b) mPW1PW91 levels.

they speculated that this difference is due to the slow regeneration, highlighting that iodine binding is not the only variable controlling V_{oc}, as described above.

More recently, Robson and co-workers have provided compelling evidence that a sluggish regeneration can lower V_{oc} [52]. They synthesized two donor–acceptor organic dyes that differ only by a two-heteroatom change from an O to S atom within the donor unit, (*E*)-3-(5-(4-(bis(4-(hexyloxy)phenyl)amino)-phenyl)thiophen-2-yl)-2-cyanoprop-2-enoic acid (**Dye–O**) and (*E*)-3-(5-(4-(bis(4-(hexylthio)phenyl)amino)phenyl)thiophen-2-yl)-2-cyanoprop-2-enoic acid) (**Dye–S**) for DSSC employing TiO_2 and iodine/iodide. Despite similar optical and redox properties for the two dyes, a consistently higher V_{oc} of the cell was measured for **Dye–S** relative to **Dye–O**. This result is inconsistent with the commonly held view that S atoms promote charge recombination attributed to intermolecular interactions with I_2 [23,49]. Through

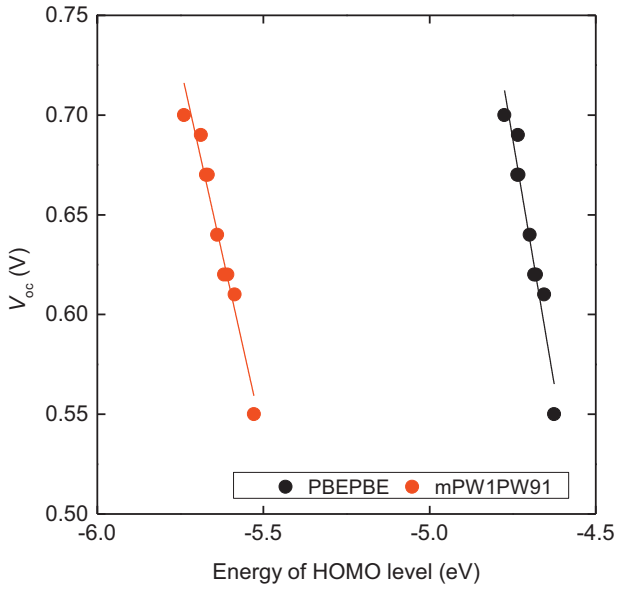

Fig. 4. Correlation between V_{oc} of the DSSC and energies of the HOMO level for neutral dyes.

detailed mechanistic studies, they concluded that this observation is a consequence of the 25-fold enhancement of the regeneration rate constant.

The key factor in the regeneration reaction of DSSC is the intermolecular interaction between the oxidized dye and I^-. Fig. 2 shows the correlation between V_{oc} (Table 1) and E of I^- for the dye^+–I^- species (Table 6). The correlation coefficients (0.94 for the L at the PBEPBE, 0.94 for the NCS at the PBEPBE, 0.91 for the L at the mPW1PW91, and 0.98 for the NCS site at the mPW1PW91 level) indicate that V_{oc} is strongly correlated to E of I^-. Fig. 3a depicts the correlation between V_{oc} (Table 1) and E value for the dye^+–I^-–I^- species at the PBEPBE level (Table 7). The correlation coefficients are 0.97 for second I^- via L, 0.97 for I_2^- via L, 0.89 for second I^- via NCS, and 0.98 for I_2^- via NCS ligand, indicating high correlations of V_{oc} with E for dye^+–I^-–I^- species at the PBEPBE level. Similar positive correlations between V_{oc} and E of the dye^+–I^-–I^- are observed at the mPW1PW91 level (Fig. 3b); the correlation coefficients are 0.98 for second I^- via L, 0.97 for I_2^- via L, 0.68 for second I^- via NCS, and 0.97 for I_2^- via NCS ligand. These findings strongly suggest that regardless if the mechanism is a one- or two-step process, the stronger the oxidized dye interacts with I^- ions, the easier the dye regeneration reaction, and the higher the V_{oc} value of DSSC.

Fig. 4 shows the correlation between V_{oc} and the energy of the HOMO level (Table 2). The correlation coefficients are 0.97 at the PBEPBE level and 0.98 at the mPW1PW91 level, indicating high correlations. As mentioned in the Introduction, the HOMO level of dye sensitizer should be more negative than the redox potential of the electrolyte, and their energy difference (ΔG_2) should allow for efficient dye regeneration. In other words, the raised HOMO energy level close to the iodine/iodide redox couple restricts the acceptance of new electrons from the redox couple [53]. The correlations observed in Fig. 4 strongly suggest that the more negative the HOMO energy level of dye and the greater the ΔG_2 value, the more efficiently the regeneration reaction and the higher V_{oc} value.

Therefore, this research confirms the hypothesis that sluggish regeneration can lower V_{oc}. Regeneration competes with the reduction of the oxidized dye by an electron from TiO_2 (electron dye recombination in Section 1) [50]. If regeneration of the oxidized dye by I^- is sluggish, reduction of dye cation by an electron from the TiO_2 instead of I^- in the electrolyte will be facilitated, leading to an inferior V_{oc} of the cell.

Listorti and co-workers have noted that it is unclear which is more important: the recombination with the electrolyte or recombination with the dye cation [54]. In case of our **FT** dyes, recombination losses with the oxidized dye during regeneration may be more dominant and important than recombination with the electrolyte because the absolute values of correlation coefficients of V_{oc} with the I^- interactions (Figs. 2–3) are larger and closer to 1 than those with I_2 interactions (Fig. 1). Judging from the correlation coefficients, recombination losses with the oxidized dye during regeneration contributes 1.4 times more to the observed change of V_{oc} than recombination with the electrolyte.

Hence, our computational results suggest that the ligand design of the sensitizer complex plays a key role in both the regeneration reaction and the recombination reaction of DSSCs.

6. Conclusions

A DFT method with full geometry optimization and subsequent population analysis reveal the remarkable effects of 2-phenylpyriminato ligand (L) in Ru(H_3tcterpy)L(NCS) dyes on the intermolecular interactions of dye with iodine molecule and iodide ions. For the nine neutral dyes, I_2 bonds to both the N atom of the L ligand and to the S atom of the NCS ligand. The V_{oc} value of DSSC decreases as the interaction strength between the neutral dye and I_2 molecule increases, irrespective of the bonding site and DFT level. The stronger the interaction of the neutral dye with I_2, the more the recombination reaction of electrons in the TiO_2 with acceptors in the electrolyte is catalyzed, reducing the V_{oc}.

I^- interacts with the oxidized dye via both the L ligand and NCS ligand. A second I^- bonds to the first I^-. These findings suggest that the regeneration of oxidized Ru(H_3tcterpy)L(NCS) dyes by I^- proceeds via the one-step and/or two-step mechanisms through a [$Dye^+ \cdot I^-$] intermediate. Contrary to the I_2 molecule, V_{oc} decreases as the interaction strength between the oxidized dye and iodides decreases. Additionally, the V_{oc} decreases as the energy of the HOMO level for the neutral dyes become more positive. The weaker the interaction of the oxidized dye with the iodide, the less efficient the dye regeneration. The more positive the HOMO level of the dye, the less the energy difference with iodine/iodide redox potential of the electrolyte (ΔG_2), leading to sluggish regeneration of oxidized dye. The sluggish regeneration facilitates the reduction of oxidized dye by an electron from the TiO_2 instead by I^- in the electrolyte, which lowers V_{oc}.

To improve V_{oc} of DSSCs, both the recombination with the electrolyte and the regeneration of dye must be considered. These results will pave the way for the design of innovative and more efficient Ru complex sensitizers.

Acknowledgments

This research was partly supported by the Japan Society for the Promotion of Science (JSPS) through its “Funding Program for World-Leading Innovative R&D on Science and Technology (FIRST Program)”. Theoretical calculations were partly performed using the Research Center for Computational Science, Okazaki, Japan.

Appendix A. Supplementary data

Supplementary data associated with this article can be found, in the online version, at http://dx.doi.org/10.1016/j.jphotochem.2013.09.001.

References

[1] B.C. O'Regan, M. Grätzel, A low-cost, high-efficiency solar cell based on dye-sensitized colloidal TiO_2 films, Nature 353 (1991) 737–740.

[2] A.N.M. Green, R.E. Chandler, S.A. Haque, J. Nelson, J.R. Durrant, Transient absorption studies and numerical modeling of iodine photoreduction by nanocrystalline TiO_2 films, J. Phys. Chem. B 109 (2005) 142–150.
[3] J.R. Jennings, Y. Liu, Q. Wang, Efficiency limitations in dye-sensitized solar cells caused by inefficient sensitizer regeneration, J. Phys. Chem. C 115 (2011) 15109–15120.
[4] C.E. Richards, A.Y. Anderson, S. Martiniani, C.H. Law, B.C. O'Regan, The mechanism of iodine reduction by TiO_2 electrons and the kinetics of recombination in dye-sensitized solar cells, J. Phys. Chem. Lett. 3 (2012) 1980–1984.
[5] X. Li, A. Reynal, P. Barnes, R. Humphry-Baker, S.M. Zakeeruddin, F. De Angelis, B.C. O'Regan, Measured binding coefficients for iodine and ruthenium dyes; implications for recombination in dye sensitized solar cells, Phys. Chem. Chem. Phys. 14 (2012) 15421–15428.
[6] A.Y. Anderson, P.R.F. Barnes, J.R. Durrant, B.C. O'Regan, Quantifying regeneration in dye-sensitized solar cells, J. Phys. Chem. C 115 (2011) 2439–2447.
[7] S. Ardo, G.J. Meyer, Photodriven heterogeneous charge transfer with transition-metal compounds anchored to TiO_2 semiconductor surfaces, Chem. Soc. Rev. 38 (2009) 115–164.
[8] J.N. Clifford, E. Martinez-Ferrero, A. Viterisi, E. Palomares, Sensitizer molecular structure-device efficiency relationship in dye sensitized solar cells, Chem. Soc. Rev. 40 (2011) 1635–1646.
[9] T. Funaki, H. Funakoshi, O. Kitao, N. Onozawa-Komatsuzaki, K. Kasuga, K. Sayama, H. Sugihara, Cyclometalated ruthenium(II) complexes as near-IR sensitizers for high efficiency dye-sensitized solar cells, Angew. Chem. Int. Ed. 51 (2012) 7528–7531.
[10] M.K. Nazeeruddin, P. Péchy, T. Renouard, S.M. Zakeeruddin, R. Humphry-Baker, P. Comte, P. Liska, L. Cevey, E. Costa, V. Shklover, L. Spiccia, G.B. Deacon, C.A. Bignozzi, M. Grätzel, Engineering of efficient panchromatic sensitizers for nanocrystalline TiO_2-based solar cells, J. Am. Chem. Soc. 123 (2001) 1613–1624.
[11] M.K. Nazeeruddin, M. Grätzel, Separation of linkage isomers of trithiocyanato (4,4′,4″-tricarboxy-2,2′,6,2″-terpyridine)ruthenium(II) by pH-titration method and their application in nanocrystalline TiO_2-based solar cells, J. Photochem. Photobiol. A: Chem. 145 (2001) 79–86.
[12] H. Kusama, H. Sugihara, K. Sayama, Theoretical study on the interactions between black dye and iodide in dye-sensitized solar cells, J. Phys. Chem. C 115 (2011) 9267–9275.
[13] T. Funaki, M. Yanagida, N. Onozawa-Komatsuzaki, K. Kasuga, Y. Kawanishi, H. Sugihara, A 2-quinolinecarboxylate-substituted ruthenium(II) complex as a new type of sensitizer for dye-sensitized solar cells, Inorg. Chim. Acta 362 (2009) 2519–2522.
[14] T. Funaki, M. Yanagida, N. Onozawa-Komatsuzaki, K. Kasuga, Y. Kawanishi, H. Sugihara, Efficient panchromatic sensitization of nanocrystalline TiO_2-based solar cells using 2-pyridinecarboxylate-substituted ruthenium(II) complexes, Chem. Lett. 38 (2009) 62–63.
[15] T. Funaki, M. Yanagida, N. Onozawa-Komatsuzaki, K. Kasuga, Y. Kawanishi, M. Kurashige, K. Sayama, H. Sugihara, Synthesis of a new class of cyclometallated ruthenium(II) complexes and their application in dye-sensitized solar cells, Inorg. Chem. Commun. 12 (2009) 842–845.
[16] S. Ghosh, K. Chaitanya, K. Bhanuprakash, M.K. Nazeeruddin, M. Grätzel, Electronic structures and absorption spectra of linkage isomers of trithiocyanato (4,4′,4″-Tricarboxy-2,2′:6,2″-terpyridine) ruthenium(II) complexes: a DFT study, Inorg. Chem. 45 (2006) 7600–7611.
[17] M.-X. Li, H.-X. Zhang, X. Zhou, Q.-J. Pan, H.-G. Fu, C.-C. Sun, Theoretical studies of the electronic structure and spectroscopic properties of $[Ru(Htcterpy)(NCS)_3]^{3-}$, Eur. J. Inorg. Chem. (2007) 2171–2180.
[18] A. Delgado, S. Corni, G. Goldoni, Low-lying electronic excitations and optical absorption spectra of the black dye sensitizer: a first-principles study, Theor. Chem. Acc. 131 (2012) 1115.
[19] H. Kusama, K. Sayama, Effect of side groups for ruthenium bipyridyl dye on the interactions with iodine in dye-sensitized solar cells, J. Phys. Chem. C 116 (2012) 1493–1502.
[20] T. Privalov, G. Boschloo, A. Hagfeldt, P.H. Svensson, L. Kloo, A study of the interactions between I^-/I_3^- redox mediators and organometallic sensitizing dyes in solar cells, J. Phys. Chem. C 113 (2009) 783–790.
[21] F. Schiffmann, J. VandeVondele, J. Hutter, A. Urakawa, R. Wirz, A. Baiker, An atomistic picture of the regeneration process in dye sensitized solar cells, Proc. Natl. Acad. Sci. U.S.A. 107 (2010) 4830–4833.
[22] M.G. Lobello, S. Fantacci, F. De Angelis, Computational spectroscopy characterization of the species involved in dye oxidation and regeneration processes in dye-sensitized solar cells, J. Phys. Chem. C 115 (2011) 18863–18872.
[23] A.M. Asaduzzaman, G.A.G. Chappellaz, G. Schreckenbach, Relationship between dye–iodine binding and cell voltage in dye-sensitized solar cells: a quantum-mechanical look, J. Comput. Chem. 33 (2012) 2492–2497.
[24] J. Nyhlen, G. Boschloo, A. Hagfeldt, L. Kloo, T. Privalov, Regeneration of oxidized organic photo-sensitizers in Grätzel solar cells: quantum-chemical portrait of a general mechanism, ChemPhysChem 11 (2010) 1858–1862.
[25] M. Zhang, J. Liu, Y. Wang, D. Zhou, P. Wang, Redox couple related influences of π-conjugation extension in organic dye-sensitized mesoscopic solar cells, Chem. Sci. 2 (2011) 1401–1406.
[26] M. Pastore, E. Mosconi, F. De Angelis, Computational investigation of dye–iodine interactions in organic dye-sensitized solar cells, J. Phys. Chem. C 116 (2012) 5965–5973.
[27] J.N. Clifford, E. Martínez-Ferrero, E. Palomares, Dye mediated charge recombination dynamics in nanocrystalline TiO_2 dye sensitized solar cells, J. Mater. Chem. 22 (2012) 12415–12422.
[28] J. Zhang, H.-B. Li, Y. Geng, S.-Z. Wen, R.-L. Zhong, Y. Wu, Q. Fu, Z.-M. Su, Modification on C219 by coumarin donor toward efficient sensitizer for dye sensitized solar cells: a theoretical study, Dyes Pigment 99 (2013) 127–135.
[29] H. Kusama, K. Sayama, Theoretical study on the intermolecular interactions of black dye dimers and black dye–deoxycholic acid complexes in dye-sensitized solar cells, J. Phys. Chem. C 116 (2012) 23906–23914.
[30] M.J. Frisch, G.W. Trucks, H.B. Schlegel, G.E. Scuseria, M.A. Robb, J.R. Cheeseman, G. Scalmani, V. Barone, B. Mennucci, G.A. Petersson, H. Nakatsuji, M. Caricato, X. Li, H.P. Hratchian, A.F. Izmaylov, J. Bloino, G. Zheng, J.L. Sonnenberg, M. Hada, M. Ehara, K. Toyota, R. Fukuda, J. Hasegawa, M. Ishida, T. Nakajima, Y. Honda, O. Kitao, H. Nakai, T. Vreven, J.A. Montgomery Jr., J.E. Peralta, F. Ogliaro, M. Bearpark, J.J. Heyd, E. Brothers, K.N. Kudin, V.N. Staroverov, R. Kobayashi, J. Normand, K. Raghavachari, A. Rendell, J.C. Burant, S.S. Iyengar, J. Tomasi, M. Cossi, N. Rega, J.M. Millam, M. Klene, J.E. Knox, J.B. Cross, V. Bakken, C. Adamo, J. Jaramillo, R. Gomperts, R.E. Stratmann, O. Yazyev, A.J. Austin, R. Cammi, C. Pomelli, J.W. Ochterski, R.L. Martin, K. Morokuma, V.G. Zakrzewski, G.A. Voth, P. Salvador, J.J. Dannenberg, S. Dapprich, A.D. Daniels, Ö. Farkas, J.B. Foresman, J.V. Ortiz, J. Cioslowski, D.J. Fox, Gaussian 09, Revision C. 01, Gaussian, Inc., Wallingford CT, 2009.
[31] J.P. Perdew, K. Burke, M. Ernzerhof, Generalized gradient approximation made simple, Phys. Rev. Lett. 77 (1996) 3865–3868.
[32] Z.Y. Li, H.L. Wang, T.J. He, F.C. Liu, D.M. Chen, Theoretical study on the structure and UV–visible spectrum of pyridine–chloranil charge-transfer complex, THEOCHEM 778 (2006) 69–76.
[33] C. Adamo, V. Barone, Exchange functionals with improved long-range behavior and adiabatic connection methods without adjustable parameters: the mPW and mPW1PW models, J. Chem. Phys. 108 (1998) 664–675.
[34] L. Pejov, M. Solimannejad, V. Stefov, The π-type hydrogen bond with triple C—C bond acting as a proton-acceptor. A gradient-corrected hybrid HF-DFT and MP2 study of the phenol–acetylene dimer in the neutral S_0 ground state, Chem. Phys. 323 (2006) 259–270.
[35] P.A. Karr, M.E. Zandler, M. Beck, J.D. Jaeger, A.L. McCarty, P.M. Smith, F. D'Souza, Predicting the site of electron transfer using DFT frontier orbitals: studies on porphyrin attached either to quinone or hydroquinone, and quinhydrone self-assembled supramolecular complexes, THEOCHEM 765 (2006) 91–103.
[36] W.J. Hehre, R. Ditchfield, J.A. Pople, Self-consistent molecular orbital methods. XII. Further extensions of Gaussian-type basis sets for use in molecular orbital studies of organic molecules, J. Chem. Phys. 56 (1972) 2257–2261.
[37] T.H. Dunning, P.J. Hay, in: Schaefer H.F.III (Ed.), Modern Theoretical Chemistry 3, Plenum, New York, 1976, pp. 1–28.
[38] P.J. Hay, W.R. Wadt, Ab initio effective core potentials for molecular calculations. Potentials for the transition metal atoms Sc to Hg, J. Chem. Phys. 82 (1985) 270–283.
[39] W.R. Wadt, P.J. Hay, Ab initio effective core potentials for molecular calculations. Potentials for main group elements Na to Bi, J. Chem. Phys. 82 (1985) 284–298.
[40] P.J. Hay, W.R. Wadt, Ab initio effective core potentials for molecular calculations. Potentials for K to Au including the outermost core orbitals, J. Chem. Phys. 82 (1985) 299–310.
[41] M. Cossi, N. Rega, G. Scalmani, V. Barone, Energies, structures, and electronic properties of molecules in solution with the C-PCM solvation model, J. Comput. Chem. 24 (2003) 669–681.
[42] F.L. Hirshfeld, Bonded-atom fragments for describing molecular charge densities, Theor. Chem. Acc. 44 (1977) 129–138.
[43] J.P. Ritchie, Electron density distribution analysis for nitromethane, nitromethide, and nitramide, J. Am. Chem. Soc. 107 (1985) 1829–1837.
[44] J.P. Ritchie, S.M. Bachrach, Some methods and applications of electron density distribution analysis, J. Comp. Chem. 8 (1987) 499–509.
[45] J.P. Foster, F. Weinhold, Natural hybrid orbitals, J. Am. Chem. Soc. 102 (1980) 7211–7218.
[46] A.E. Reed, L.A. Curtiss, F. Weinhold, Intermolecular interactions from a natural bond orbital, donor–acceptor viewpoint, Chem. Rev. 88 (1988) 899–926.
[47] J.N. Clifford, E. Palomares, M.K. Nazeeruddin, M. Grätzel, J.R. Durrant, Dye dependent regeneration dynamics in dye sensitized nanocrystalline solar cells: evidence for the formation of a ruthenium bipyridyl cation/iodide intermediate, J. Phys. Chem. C 111 (2007) 6561–6567.
[48] J.M. Gardner, J.M. Giaimuccio, G.J. Meyer, Evidence for iodine atoms as intermediates in the dye sensitized formation of I—I bonds, J. Am. Chem. Soc. 130 (2008) 17252–17253.
[49] B.C. O'Regan, K. Walley, M. Juozapavicius, A. Anderson, F. Matar, T. Ghaddar, S.M. Zakeeruddin, C. Klein, J.R. Durrant, Structure/function relationships in dyes for solar energy conversion: a two-atom change in dye structure and the mechanism for its effect on cell voltage, J. Am. Chem. Soc. 131 (2009) 3541–3548.
[50] B.C. O'Regan, J.R. Durrant, Kinetic and energetic paradigms for dye-sensitized solar cells: moving from the ideal to the real, Acc. Chem. Res. 42 (2009) 1799–1808.

[51] J.R. Jennings, Y. Liu, Q. Wang, S.M. Zakeeruddin, M. Grätzel, The influence of dye structure on charge recombination in dye-sensitized solar cells, Phys. Chem. Chem. Phys. 13 (2011) 6637–6648.
[52] K.C.D. Robson, K. Hu, G.J. Meyer, C.P. Berlinguette, Atomic level resolution of dye regeneration in the dye-sensitized solar cell, J. Am. Chem. Soc. 135 (2013) 1961–1971.
[53] H. Kusama, H. Sugihara, K. Sayama, Nitrogen-containing heterocycles' interaction with Ru dye in dye-sensitized solar cells, J. Phys. Chem. C 113 (2009) 20764–20771.
[54] A. Listorti, B.C. O'Regan, J.R. Durrant, Electron transfer dynamics in dye-sensitized solar cells, Chem. Mater. 23 (2011) 3381–3399.